ARTICLE

Ab initio Potential Energy Surfaces and Low–Temperature Collisional Dynamics for Rotational De-excitation of HNC and HCN by Ar

Liman Tian[a], Tong Sun[a], Chuangang Ning[b], Xiaolin Chen[a*]

a. College of Optical, Mechanical and Electrical Engineering, Zhejiang Agriculture and Forestry University, Hangzhou 311300, China
b. State Key Laboratory of Low-Dimensional Quantum Physics, Department of Physics, Tsinghua University, Beijing 10084, China

(Dated: Received on January 5, 2026; Accepted on January 26, 2026)

Accurate modeling of nitrogen-rich atmospheres, such as that of Titan, requires precise collisional data with key secondary partners such as Ar. This work presents a quantum scattering investigation of rotational (de-)excitation of HCN and HNC molecules in their ground vibrational state in collisions with Ar. Two-dimensional potential energy surfaces were constructed using the CCSD(T)-F12A/aug-cc-pVTZ method, achieving accuracy near the complete basis set limit. State-to-state integral cross-sections for rotational transitions were computed by solving the quantum close-coupling equations for all rotational quantum number $j \leq 8$, over collision energies up to 1000 cm^{-1}, and were then thermally averaged to obtain de-excitation rate coefficients for temperatures of 5–200 K. A propensity rule for clear rate coefficients is observed: in contrast to the HCN–He system, which favors even Δj transitions, the HCN–Ar system exhibits a strong propensity for odd Δj transitions at $j < 4$ and for even transitions at $j \geq 4$. This propensity gradually weakens at higher temperatures but remains observable. The provided rate coefficients supply essential data for astrochemical models involving Ar, enabling more accurate treatment of HCN/HNC (de-)excitation and radiative transfer in interstellar and planetary environments, thereby improving the reliability of derived molecular abundance ratios.

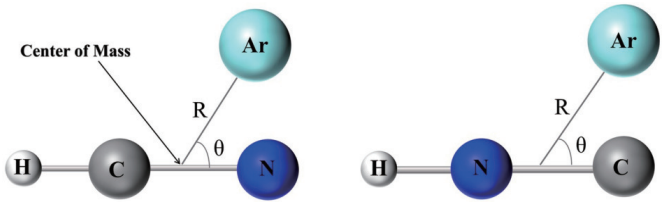

Key words: Potential energy surface, Inelastic rotational collision, Close coupling, Cross section, Rate coefficient

I. INTROUCTION

The dense atmosphere of Titan, composed predominantly of N_2 and CH_4, sustains a complex organic chemistry that leads to the formation of nitriles [1, 2]. Hydrogen cyanide (HCN), first detected in Titan's atmosphere by the Voyager mission [3], is a critical product of photochemical and ion-molecule processes [4]. Its unstable isomer, HNC, which was later detected in Titan's atmosphere via its rotational transition $J=6\rightarrow5$ by Moreno *et al.* [5], also serves as a precursor to more complex organic compounds [1, 6–8]. The HNC/HCN abundance ratio provide a powerful diagnostic for understanding chemical pathways and isomer-specific processes in Titan's atmosphere [9–11]. Consequently, accurate radiative transfer modeling of HNC and HCN, which is essential for interpreting observational data, requires precise collisional rate coefficients with the dominant atmospheric species.

In the interstellar medium (ISM), the HNC/HCN

* Author to whom correspondence should be addressed.
E-mail: chenxl13@zafu.edu.cn

abundance ratio correlates strongly with temperature [12, 13]. In very cold environments, HNC appears more abundant than HCN, which is a counterintuitive result that has long intrigued astronomers [14]. Rotational (de-)excitation of HCN and HNC is commonly modeled using collisional data with He or H_2. Recent experimental work by Hay *et al.* [11] has confirmed earlier quantum scattering studies [15, 16], showing that due to differences in the anisotropy of their interaction potentials, the HCN−He and HNC−He systems exhibit fundamentally different collisional de-excitation behaviors: HCN−He favors even Δj transitions, whereas HNC−He favors odd Δj transitions. These differences significantly affect the inferred HNC/HCN abundance ratio, demonstrating that using HCN collisional data as a proxy for HNC may lead to substantial biases [15]. In particular, Sarrasin *et al.* [16] showed that in cold dark clouds, the HNC/HCN abundance ratio derived from observations has to be revised from >1 to ≈ 1 due to these collisional differences.

Previous studies of collisions with He have shown that the collisional excitation process is highly sensitive to molecular isomerism. This strong dependence motivates the extension of such investigations to systems involving heavier partners. Although N_2 is the dominant species in Titan's atmosphere, Ar, being the most abundant noble gas present [17, 18], serves as a crucial benchmark for studying heavy particle collision dynamics. Its interaction properties are fundamentally distinct from those of the light partners prevalent in the ISM, such as He or H_2. Early experimental evidence from microwave double resonance studies of HCN with rare gases indicates that the patterns of collision-induced rotational transitions for Ar (and Xe) differ qualitatively from those of He [19], highlighting the importance of the perturber's polarizability and mass. While prior theoretical studies have provided initial insights into the HCN/HNC−Ar systems [20–22], state-to-state rotational (de-)excitation data based on high-level *ab initio* potential energy surfaces (PESs) and exact quantum scattering methods at low temperatures remain unavailable. Consequently, approximating rates for Titan's conditions using coefficients derived from He or H_2 collisions may lead to significant inaccuracies. Indeed, using H_2 or He as proxies may not fully capture the detailed collisional dynamics of the N_2/CH_4/Ar atmospheric mixture on Titan. This conclusion is corroborated by studies of other molecular systems, demonstrating that rate coefficients for H_2 collisions cannot be accurately obtained by a simple scaling method of He collision coefficients, due to fundamental differences in the underlying interaction potentials [23, 24].

This paper utilizes Ar to establish a fundamental benchmark for collisions involving heavy atomic partners with HNC and HCN. Section II details the computational methodology, including the construction of the HNC−Ar and HCN−Ar PESs using the CCSD(T)-F12A method and a comparison of this approach with the highly accurate CCSD(T)/CBS benchmark. We also describe the use of Gauss–Legendre quadrature to compute the radial coefficients of the potentials. Section III presents the results of quantum close-coupling calculations, providing integral cross-sections for rotational de-excitation and thermal rate coefficients spanning the temperature range of 5–200 K. By systematically comparing the collisional behavior of HCN−Ar and HNC−Ar, we elucidate the differences in their transition propensities. Section IV summarizes our findings and conclusions.

II. COMPUTATIONAL DETAILS

A. Potential energy surfaces

The interaction potentials of the HNC−Ar and HCN−Ar complexes were calculated within the rigid-rotor approximation, considering both molecules in their electronic ground state ($X^1\Sigma^+$) and Ar in the ^1S state. This approximation is well suited to the low-energy regime under consideration because intramolecular vibrations have only a minor influence on cross-sections for pure rotational excitation, as established in earlier studies [15, 16, 25]. Although strong vibration-rotation coupling can occur in non-rigid polyatomic molecules, linear triatomic species such as HNC and HCN possess relatively rigid geometries. In the energy range relevant to rotational excitation, these molecules lack large-amplitude soft bending or torsional modes. Their spectroscopic signatures, characterized by well-separated rotational and vibrational lines, are consistent with the rigid-rotor model.

As illustrated for the HCN−Ar system in FIG. 1, a Jacobi coordinate system was used in the calculations. Here, R represents the distance from the center of mass of the molecule (HNC or HCN) to Ar, and θ denotes the angle between the molecular axis and the vector $\boldsymbol{R}$. For the HCN−Ar system, $\theta = 0°$ corresponds to the linear

DOI: 10.1063/1674-0068/cjcp2601003

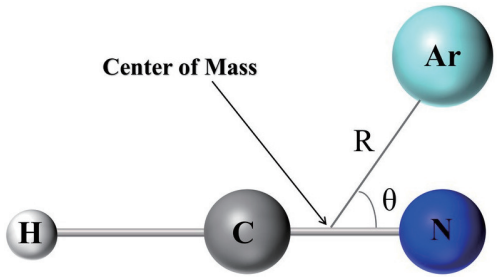

FIG. 1 Jacobian coordinates for the HCN ($(X^1\Sigma^+)$–Ar (^1S)) collisional system.

HCN–Ar configuration, and $\theta = 180°$ to Ar–HNC configuration. The molecular geometries were fixed at their experimental ground-state equilibrium structures: $r_{NH} = 0.994$ Å and $r_{NC} = 1.169$ Å for HNC [26]; $r_{CH} = 1.065$ Å and $r_{CN} = 1.153$ Å for HCN [27].

PESs for the HNC/HCN–Ar van der Waals systems were computed using the explicitly correlated coupled cluster singles, doubles, and perturbative triples, augmented by explicitly correlated functions (CCSD(T)-F12A) method [28]. The aug-cc-pVTZ basis set was employed for all atoms (H, C, N, and Ar) [29, 30]. For both systems, the counterpoise procedure of Boys and Bernardi [31] was applied to correct for basis set superposition error (BSSE):

$$V(R,\theta) = E_{\mathrm{HX-Ar}}(R,\theta) - E_{\mathrm{HX}}(R,\theta) - E_{\mathrm{Ar}}(R,\theta) \quad (1)$$

Here, HX denotes HCN or HNC. $V(R, \theta)$ represents the interaction potential for the HX–Ar complex. $E_{\mathrm{HX-Ar}}$, E_{HX}, and E_{Ar} are the total energies of the HX–Ar, HX, and Ar monomers, respectively. For each PES, a total of 1767 *ab initio* energy points were computed, providing extensive sampling of the configuration space that includes the equilibrium, short-range repulsive, and long-range asymptotic regions. The intermonomer distance R was sampled from 2.5 Å to 30.0 Å, and the angle θ was varied in 10° increments from 0° to 180°.

The calculated PESs for HCN–Ar and HNC–Ar are presented in FIG. 2 (a) and (b), respectively. FIG. 2(a) features a single global minimum located at $R = 4.496$ Å and θ=180° for the HCN–Ar system, corresponding to a linear Ar–HCN geometry with a well depth of 144.91 cm^{-1}. For the HNC–Ar system, its global minimum occurs at R=4.133 Å and θ=180°, corresponding to a linear Ar–HNC geometry with a well depth of 222.02 cm^{-1}. The HNC–Ar well depth is substantially greater than that of the HNC–He system (≈46.83 cm^{-1}) [16]. A similar enhancement in well depth is observed for the

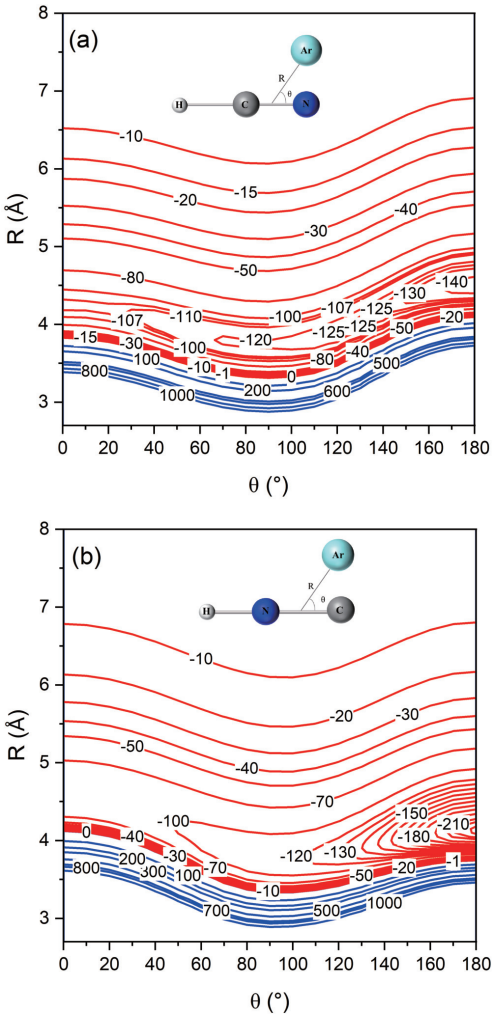

FIG. 2 Contour plots of the PESs for (a) HCN–Ar and (b) HNC–Ar as functions of the intermolecular distance R and angular coordinate θ. Energy values are given in cm^{-1}. The negative energy regions are denoted by red contours, while the positive energy regions are represented by blue contours.

HCN–Ar relative to HCN–He. This marked enhancement in the well depths is primarily due to the electric dipole polarizability of Ar, which is approximately eight times greater than that of He [32]. This greater polarizability strengthens the induction and dispersion interactions, leading to significantly deeper potential wells of both the HCN–Ar and HNC–Ar systems.

To assess the accuracy of the CCSD(T)-F12A/aug-cc-pVTZ (AVTZ) method for these systems, we computed one-dimensional (1D) potential energy curves along the angular coordinate at θ=180° for both HNC–Ar and HCN–Ar. For completeness, similar calculations were performed at other characteristic angles (θ=0°, 90°), which consistently confirmed the performance of the method. As shown in FIG. 3, the potential

DOI: 10.1063/1674-0068/cjcp2601003

TABLE I Potential energy of the HNC−Ar and HCN−Ar systems for the linear arrangement θ=180° computed at different levels of theory as a function of R.

Theory level	HNC−Ar potential energy/cm^{-1}			HCN−Ar potential energy/cm^{-1}		
	R=4.10 Å	R=4.20 Å	R=4.30 Å	R=4.40 Å	R=4.50 Å	R=4.60 Å
CCSD(T)/AVTZ	–198.65	–200.57	–191.88	–121.00	–129.00	–128.00
CCSD(T)/AVQZ	–217.26	–215.83	–204.48	–137.00	–142.00	–142.00
CCSD(T)/AV5Z	–221.39	–219.11	–207.23	–141.00	–145.00	–142.00
CCSD(T)/CBS	–223.76	–220.99	–208.81	–143.31	–146.73	–143.73
CCSD(T)–F12A/AVTZ	–221.30	–219.04	–207.06	–140.00	–145.00	–141.00
CCSD(T)–F12B/AVQZ	–220.99	–218.81	–206.97	–140.72	–145.35	–141.48

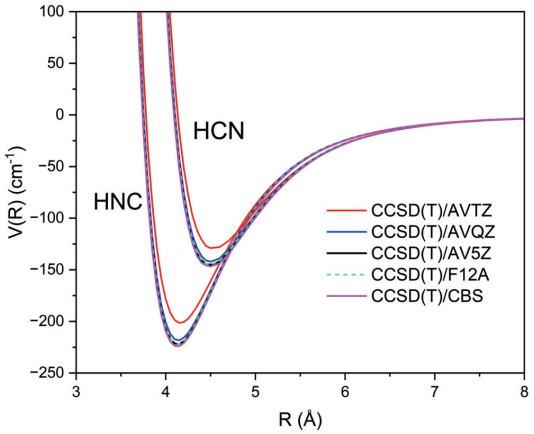

FIG. 3 1D PESs of HNC−Ar and HCN−Ar at θ=180°. The curves were calculated using CCSD–F12A/AVTZ and CCSD(T) methods with different basis sets and CBS extrapolation.

energy curves obtained with the CCSD(T)-F12A/AVTZ method are in excellent agreement with those derived from the complete basis set (CBS) limit. The CBS limit values were obtained via a three-parameter exponential extrapolating [33] of conventional CCSD(T)/aug-cc-pVXZ (X = T, Q, 5) method. A quantitative comparison is provided in Table I. The CCSD(T)-F12A/AVTZ interaction energies deviate by less than 1% from the CBS limit values, demonstrating accuracy comparable to that of the much more computationally expensive CCSD(T)/aug-cc-pV5Z level of theory. Although the alternative CCSD(T)-F12B variant offers comparable accuracy, the CCSD(T)-F12A approach was selected for its superior computational efficiency, providing an optimal balance between accuracy and resource expenditure for constructing the extensive PESs required in this work. The reliability of this computational approach is further supported by its successful application in accurately describing other van der Waals complexes, such as OCS−Ar [34], O_3−Ar [35], and HNSi−He [36]. All *ab initio* calculations were carried out using the MOLPRO quantum chemistry package [37].

B. Analytical representation

The PESs for the HCN−Ar and HNC−Ar systems were expressed via a standard Legendre polynomial expansion [38] for the subsequent quantum scattering calculations. The potential is expressed as:

$$V(R,\theta) = \sum_{\lambda=0}^{\lambda_{\max}} V_\lambda(R) P_\lambda(\cos\theta) \tag{2}$$

where P_λ (cosθ) denotes the Legendre polynomial of order λ. The corresponding radial expansion coefficients $V_\lambda(R)$ were obtained via Gauss−Legendre quadrature with 17 integration points:

$$V_\lambda(R) = \left(\frac{2\lambda+1}{2}\right) \int_0^\pi V(R,\theta) P_\lambda(\cos\theta) \sin\theta \mathrm{d}\theta \tag{3}$$

The expansion was truncated at $\lambda_{\max}$ =14 and 15 for HNC−Ar and HCN−Ar. This truncation ensures a relative error of less than 0.5% between the analytically fitted potential and the *ab initio* points across the entire configuration space.

FIG. 4 displays the radial coefficients $V_\lambda(R)$ for λ = 0−3 as functions of R for HNC−Ar (solid lines) and HCN−Ar (dashed lines). For HCN−Ar, the anisotropy is dominated by the λ = 2 term, reflecting an approximate symmetry under end-for-end interchange ($\theta \to \pi-\theta$). In contrast, the HNC–Ar potential in the key interaction region (approximately 3.9−4.2 Å) is characterized by dominant contributions from the λ = 1 and 3 terms. This dominance of odd-order terms reflects a pronounced odd anisotropy in the PES, a direct consequence of the molecule's intrinsic asymmetry, consis-

DOI: 10.1063/1674-0068/cjcp2601003

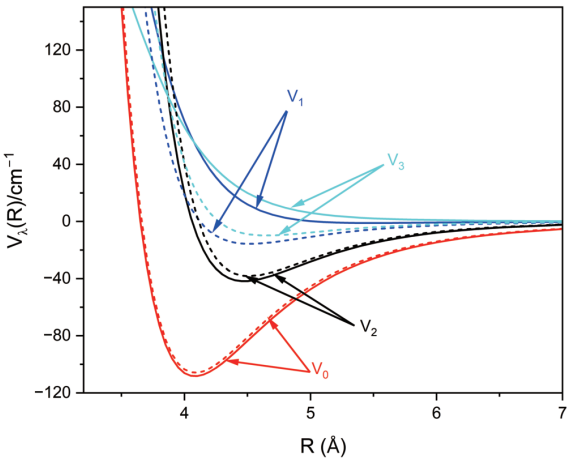

FIG. 4 Plot of first four radial Legendre expansion coefficients (λ=0–3) as a function of R. Solid lines denote HNC–Ar, and dashed lines denote HCN–Ar.

tent with findings for the HNC–He system [16]. At larger separations (4.0–5 Å), the λ=2 term also becomes significant for HNC–Ar. Interestingly, for HCN–Ar around R≈4 Å, the magnitude of the V_3 briefly exceeds that of V_2. This subtle feature, less pronounced in the corresponding He complexes, may arise from enhanced induction interactions due to the high polarizability of Ar, which can more strongly couple with the permanent electric moments of the HCN molecule.

Following the procedure of Ajili and Hammami for long-range representation, the asymptotic form of the interaction was explicitly incorporated into the analytical potential fit [39]. FIG. 5(a) compares the *ab initio* points, the isotropic coefficient $V_0(R)$, the CBS limit, and the final analytical potential for the linear HCN–Ar ($\theta = 0°$) configuration. An analogous comparison for the linear HNC–Ar (θ=0°) configuration is presented in FIG. 5 (b). Excellent agreement is observed in both cases. As shown in FIG. 5, the interaction energies computed at the CCSD(T)-F12A/AVTZ level are in excellent agreement with the CBS limit. This confirms that the CCSD(T)-F12A/AVTZ method provides an optimal balance, delivering accuracy near the CBS limit while substantially reducing computational cost. Moreover, the consistency between the fitted potentials and the *ab initio* data across all sampled geometries confirms the robustness of the fitting protocol. A critical aspect of the fitting process is the enforcement of the correct asymptotic behavior. In the long-range region, where dispersion interactions dominate, the potential must converge to the theoretical $-C_6/R^6$ form. FIG. 5 shows that the fitted isotropic radial coefficient, $V_0(R)$, successfully reproduces the *ab initio* points and seamlessly

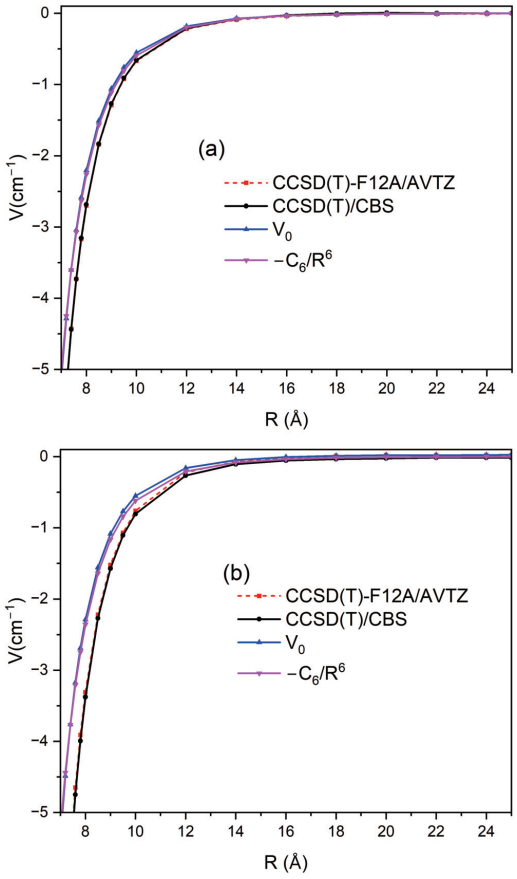

FIG. 5 Comparison between the long-range *ab initio* and analytical potential energies of (a) HCN–Ar system and (b) HNC–Ar system at θ=0°.

merges with the $-C_6/R^6$ curve at large internuclear separations. This successful integration of the physically correct asymptotic form into the global fit ensures the reliability of the PES, particularly in the long-range region. An accurate description of this region is essential for converging quantum scattering calculations, as it influences resonance positions and the convergence of integral cross-sections.

III. RESULTS AND DISCUSSION

A. Inelastic cross-sections

The quantum dynamics of inelastic scattering in the HNC/HCN–Ar system is treated within the close-coupling method, initially developed by Arthur and Dalgarno [40]. The integral cross section $\sigma_{j\to j'}(E_k)$, which depends on the collision energy for the molecule, is obtained by summing the reaction probabilities over all values of the total angular momentum quantum number J, given by Green [41] in the form of the scattering matrix $S^J_{jj',ll'}$:

DOI: 10.1063/1674-0068/cjcp2601003

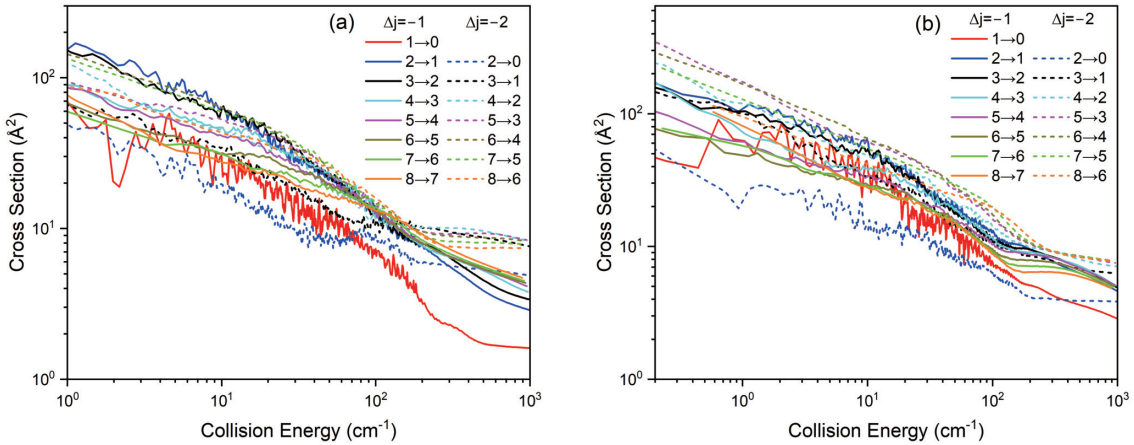

FIG. 6 Inelastic state-to-state cross-sections (in units of Å^2) as a function of collision energy for de-excitation of (a) HNC and (b) HCN with Ar.

$$\sigma_{j\to j'}(E_k) = \frac{\pi}{k_j{}^2(2j+1)} \sum_{J=0} \sum_{l=|J-j|}^{J+j} \sum_{l'=|J-j'|}^{J+j'} \times (2J+1) \left|\delta_{jj'}\delta_{ll'} - S^J_{jj'll'}(E)\right|^2 \tag{4}$$

Here, J is the total angular momentum quantum number, j and j' are the initial and final rotational states, l and l' are the initial and final orbital momentum quantum number, and E is the total energy. The wavevector is $k_j = \sqrt{2\mu(E-E_j)}/\hbar$, and E_j is the rotational energy of state j. The rotational energy levels are described by:

$$E_j = B_0 j(j+1) - D_0[j(j+1)]^2 \tag{5}$$

Where B_0 and D_0 are the rotational and centrifugal distortion constant, respectively. The experimental values for these constants were taken from Pearson *et al.* [42] for HNC and Maki *et al.* [43] for HCN. The rigorous quantum mechanical calculations performed with MOLSCAT code [44] establish a robust basis for the subsequent computation of rotational excitation and relaxation cross-sections in the HNC−Ar and HCN−Ar systems.

Cross-sections were computed for transitions originating from all rotational levels up to $j=8$, focusing on $\Delta j=\pm1$ and $\pm$ 2 for both excitation and de-excitation processes. The calculations for the HNC/HCN−Ar systems were performed at collision energies ranging from 0 to 1000 cm^{-1} using a variable energy grid: 0.2 cm^{-1} from 0 to 80 cm^{-1}, 1.0 cm^{-1} from 80 cm^{-1} to 200 cm^{-1}, 5.0 cm^{-1} from 200 cm^{-1} to 500 cm^{-1}, and 20.0 cm^{-1} from 500 cm^{-1} to 1000 cm^{-1}. To achieve convergence for cross-sections involving levels up to $j=8$, the rotational basis cutoff J_{max} was optimized for each system and collision energy range. For HNC–Ar, the values were $J_{max}=15$ ($E\leq100$ cm^{-1}), $J_{max}=17$ (100 cm$^{-1}<E\leq300$ cm^{-1}), $J_{max}=20$ (300 cm$^{-1}<E\leq500$ cm^{-1}), and $J_{max}=25$ (500 cm$^{-1}<E\leq1000$ cm^{-1}). For HCN–Ar, $J_{max}=15$ ($E\leq100$ cm^{-1}), $J_{max}=20$ (100 cm$^{-1}<E\leq500$ cm^{-1}), and $J_{max}=27$ (500 cm$^{-1}<E\leq1000$ cm^{-1}). The number of steps per de Broglie wavelength for numerical integration was set to 20 for $E<100$ cm^{-1}, and 10 for $E>100$ cm^{-1}. The total angular momentum, J_{tot} (JTOTU in the code), was automatically converged for each collision energy, with a maximum allowed value of 99999. The off-diagonal and diagonal convergence tolerances for cross-section calculations (OTOL and DTOL) were maintained at 0.001 Å^2 and 0.01 Å^2, respectively. The coupled equations were solved using the modified log-derivative method of Manolopoulos (LDMD) [45] at short range and the Airy propagator at long range [46].

FIG. 6 (a) and (b) display the rotational de-excitation cross-sections for $\Delta j=-1$ and -2 transitions in HNC−Ar and HCN−Ar, respectively. Both systems show similar energy dependence in their de-excitation cross-sections, with dense resonance structures observed at collision energies below 100 cm^{-1}. These resonances originate primarily from quasi-bound states on

DOI: 10.1063/1674-0068/cjcp2601003

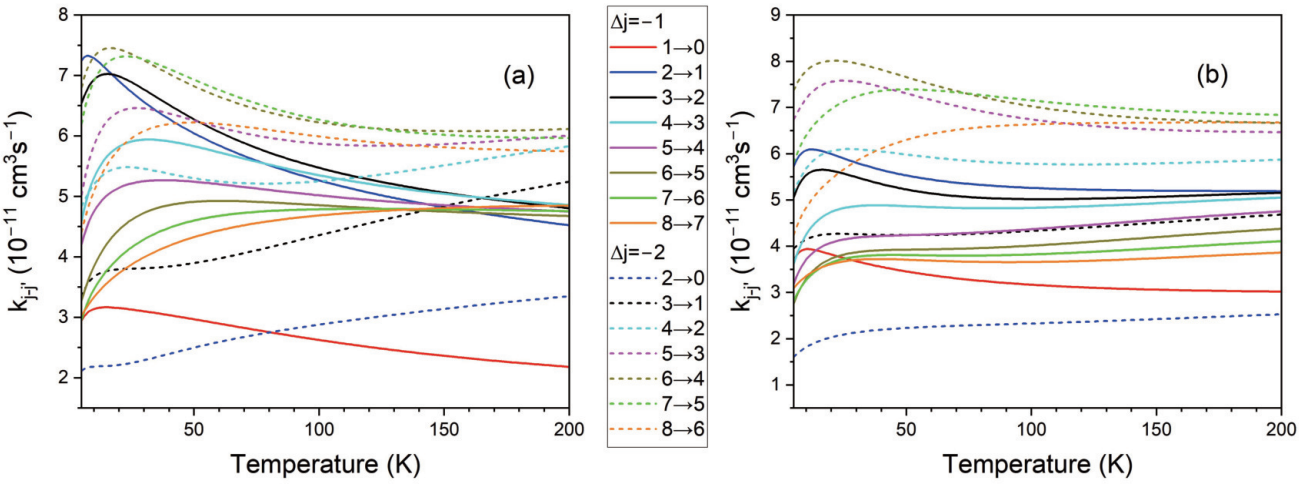

FIG. 7 State-to-state rate coefficients as a function of temperature for inelastic cross-sections as a function of collision energy for de-excitation of (a) HNC and (b) HCN in collisions with Ar.

the PESs, encompassing both shape and Feshbach resonances. As the collision energy increases above ~100 cm^{-1}, the resonance structures gradually diminish and eventually disappear. In this regime, the cross-sections decrease smoothly, indicating the dominance of a direct collision mechanism at higher energies. For initial rotational levels $j\leq3$, both systems exhibit a clear propensity for $\Delta j=-1$ transitions at collision energies below ~100 cm^{-1}. This propensity progressively weakens as the energy increases, and a reversal occurs where the scattering cross-sections for $\Delta j=-2$ become larger than that for $\Delta j=-1$. The behavior of the rotational excitation cross-sections is consistent with our recent findings on the analogous HNSi/HSiN–He systems [36]. However, due to the complexity of the collision systems, the propensity rule becomes less pronounced. The scattering trends in cross-sections do not directly correlate with the radial coefficients of the PESs, particularly at low energies. This may be attributed to differences in the anisotropy of the potential. The potential well depth for HCN−Ar is approximately four times deeper than that for HCN–He [16], leading to more pronounced resonance effects in HCN–Ar. The stronger HCN−Ar interaction enhances subtle anisotropic effects that are negligible in He collisions. Ar tends to reside deeper in the potential well near the H end, similar to its behavior in the He−HCN system. Furthermore, the larger atomic mass of Ar compared to He may enhance low-energy resonance effects and further favor odd Δj transitions in HCN–Ar collisions at low energy. Nevertheless, as shown in FIG. 6(b), at energies approaching 1000 cm^{-1}, the cross-sections for the 2→1 and 2→0 transitions become comparable, while those for 3→2 and 3→1 cross, indicating a shift toward even Δj behavior. This suggests that at sufficiently high collision energies, transitions with $j<4$ will also exhibit a preference for even Δj transitions, similar to the HCN–He system.

B. Rate coefficients

The rate coefficients for rotational de-excitation, $k_{j\to j'}(T)$, in HNC/HCN−Ar collisions are obtained via the following expression:

$$k_{j\to j'}(T)=\left(\frac{8}{\pi\mu k_{\mathrm{B}}^3T^3}\right)^{1/2}\int_0^\infty E_k\sigma_{j\to j'}(E_k)e^{-E_k/k_BT}\mathrm{d}E_k \tag{6}$$

Here, μ is the reduced mass of the respective collisional system (HNC−Ar or HCN−Ar) and k_{B} is the Boltzmann constant. Only the de-excitation rate coefficients are reported because excitation rate coefficients can be easily deduced from detailed balance [47].

FIG. 7(a) presents the de-excitation rate coefficients for $\Delta j=-1$ and −2 transitions in HNC–Ar collisions as a function of temperature in the range of 5–200 K. For initial rotational levels $j\leq4$ at temperatures below 100 K, the rate coefficients for $\Delta j=-1$ transitions consistently exceed those for $\Delta j=-2$. For $j>4$, the $\Delta j=-2$ rate coefficients remain larger than the $\Delta j=-1$ coefficients across the entire temperature range. This behavior is similar to that reported for the HNC–He system [15], in which the de-excitation rates for the 2→1 transition exceed that for 2→0, while the rate for 10→8 is

DOI: 10.1063/1674-0068/cjcp2601003

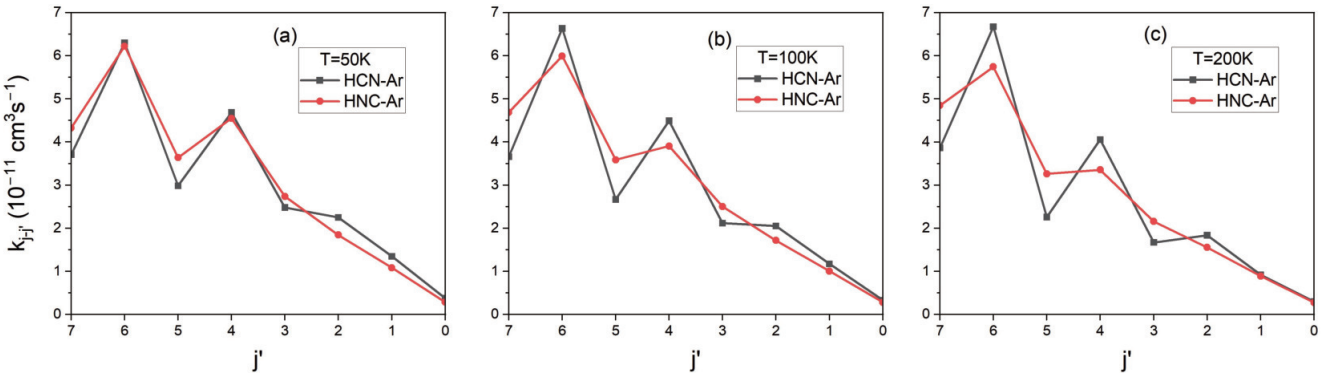

FIG. 8 HNC–Ar and HCN–Ar de-excitation rate coefficients from the initial level j=8 at (a) 50 K, (b) 100 K, and (c) 200 K, respectively. See the main text for further details.

higher than that of 10→9. Furthermore, for a specific transition such as 2→1, the rate for HNC–He is approximately four times larger than that for HNC−Ar, suggesting that de-excitation proceeds more readily in the former system. A notable inversion occurs for the transition from $j=3$ near 150 K, where the rate coefficient of 3→1 transition exceeds that for 3→2. Such a crossover is not observed in the HNC–He system [15]. FIG. 7(b) illustrates the de-excitation rate coefficients for $\Delta j=-1$ and −2 transitions in the HCN–Ar system. In contrast to HNC−Ar, the HCN−Ar system exhibits consistently larger rate coefficients for $\Delta j=-1$ than for $\Delta j=-2$ transitions across the entire temperature range for initial levels $j<4$. However, for $j\geq4$, the $\Delta j=-2$ rate coefficients are consistently larger. This differs from the propensity for even Δj transitions observed in the HCN–He system [15, 16]. The difference is attributed to the larger atomic mass and greater polarizability of the Ar collision partner compared to He.

FIG. 8 shows the de-excitation rate coefficients from the initial rotational level $j=8$ for HNC–Ar and HCN–Ar at temperatures of 50, 100, and 200 K. Significant differences are observed between the two systems, which reflect the distinct structural anisotropies of their respective PESs. At temperatures of 50 K, the rate coefficients vary smoothly without a pronounced propensity for odd or even Δj, as the low collision energies primarily sample the long-range region of the potential. As the temperature rises, a clear odd-even propensity emerges. The HNC–Ar system exhibits a strong preference for odd Δj transitions (*e.g.*, 8→7, 8→5), while the HCN–Ar system favors even Δj transitions (*e.g.*, 8→6, 8→4). This behavior mirrors the known propensity reversal between HCN and HNC in collisions with He. It originates from the different dominant anisotropic terms in their respective PES. The propensity rules weaken with a further increase in temperature for higher Δj transitions (*e.g.*, 8→1). In particular, the rate coefficients for even Δj transitions in HNC−Ar grow more rapidly than those for odd Δj, which leads to a weakening of the initial odd propensity, a behavior that is also clearly demonstrated for the HNC–He system [15]. This is due to the increasing role of short-range interactions at higher collision energies, which probes different anisotropic components of the potential. This temperature-dependent evolution implies that extrapolating low-temperature propensity rules to higher temperatures is unreliable. Accurate modeling in warm astrophysical environments therefore requires dedicated scattering calculations.

This study reveals that both HNC and HCN rate coefficients exhibit a pronounced propensity for even Δj transitions during rotational excitation by Ar at rotation levels $j\geq4$. This behavior is similar to that observed in collisions with He. As the interaction distance extends to 4–5 Å, the amplitudes of the odd-order anisotropy terms V_1 and V_3 no longer consistently dominate the PES, but instead enter a competitive relationship with the even-order term V_2. Furthermore, the higher polarizability of Ar, compared to He, leads to deeper potential wells and a corresponding enhancement of the odd-order anisotropy at low collision energy. These deeper, more anisotropic potentials not only reinforce the odd Δj propensity but also give rise to more prominent resonant structures in the cross-sections at low collision energy. Consequently, substituting He-collision data for the Ar system introduces significant systematic errors in the rate coefficients. This would severely compromise the reliability of derived molecular abundances and excitation conditions for

DOI: 10.1063/1674-0068/cjcp2601003

HCN and HNC in astrophysical modeling.

IV. CONCLUSION

In summary, this work presents a quantum scattering study of rotationally inelastic collisions between HNC/HCN and Ar, employing accurate potential energy surfaces. High-precision two-dimensional (2D) PESs for both HNC–Ar and HCN–Ar were constructed using the CCSD(T)-F12A method in conjunction with aug-cc-pVTZ basis set. This approach offers high computational efficiency while delivering accuracy near the CBS limit. The PESs reveal distinct equilibrium geometries. The global minimum for HNC−Ar is at the linear Ar−HNC configuration (R = 4.133 Å, θ = 180°) with a well depth of 222.02 cm^{-1}, whereas for HCN−Ar, it is at the linear Ar−HCN configuration (R = 4.496 Å, θ = 180°) with a depth of 144.91 cm^{-1}. Compared to HNC−Ar, the HCN−Ar PES shows a broader angular well, indicating weaker anisotropy.

The CC method was used to compute integral cross-sections for rotational de-excitation transitions with Δj = −1 and −2 up to rotational levels j=8. These cross-sections were then used to derive temperature-dependent rate coefficients for the 5−200 K range. In contrast to the HCN−He and HNC−He systems, both HNC−Ar and HCN−Ar rate coefficients exhibit a clear odd Δj propensity at temperatures up to 100 K for initial levels j<4. As the temperature and initial rotational level j increase, a propensity for even Δj transitions gradually develops. The high polarizability of Ar leads to deeper potential wells and more pronounced scattering resonances than for He, which underpins the stronger odd-Δj propensity observed at low temperatures. This study provides reliable collisional data for HNC/HCN−Ar systems, which are essential for non-LTE astrophysical modeling. Consequently, the significant influence of Ar's polarizability on the potential and dynamics underscores the necessity of using partner-specific collisional data in astrochemical simulations.

V. ACKONWLEDGMENTS

This work was supported by the National Natural Science Foundation of China (Nos. 12374244 and 12341401), and Scientific Research Development Fund Project of the Zhejiang A&F University (No.2024LFR048).

VI. CONFLICT OF INTEREST

The authors have no conflicts to disclose.

[1] C. A. Nixon, ACS Earth Space Chem. **8**, 406 (2024).
[2] S. M. Hörst, J. Geophys. Res. Planets **122**, 432 (2017).
[3] R. Hanel, B. Conrath, F. M. Flasar, V. Kunde, W. Maguire, J. Pearl, J. Pirraglia, R. Samuelson, L. Herath, M. Allison, D. Cruikshank, D. Gautier, P. Gierasch, L. Horn, R. Koppany, and C. Ponnamperuma, Science **212**, 192 (1981).
[4] V. Vuitton, R. V. Yelle, S. J. Klippenstein, S. M. Hörst, and P. Lavvas, Icarus **324**, 120 (2019).
[5] R. Moreno, E. Lellouch, L. M. Lara, R. Courtin, D. Bockelée-Morvan, P. Hartogh, M. Rengel, N. Biver, M. Banaszkiewicz, and A. González, Astron. Astrophys. **536**, L12 (2011).
[6] M. Rahm, J. I. Lunine, D. A. Usher, and D. Shalloway, Proc. Natl. Acad. Sci. USA **113**, 8121 (2016).
[7] K. Willacy, M. Allen, and Y. Yung, Astrophys. J. **829**, 79 (2016).
[8] B. K. D. Pearce, P. W. Ayers, and R. E. Pudritz, J. Phys. Chem. A **123**, 1861 (2019).
[9] E. Hébrard, M. Dobrijevic, J. C. Loison, A. Bergeat, and K. M. Hickson, Astron. Astrophys. **541**, A21 (2012).
[10] A. Aguado, O. Roncero, A. Zanchet, M. Agúndez, and J. Cernicharo, Astrophys. J. **838**, 33 (2017).
[11] B. M. Hays, D. Gupta, T. Guillaume, O. Abdelkader Khedaoui, I. R. Cooke, F. Thibault, F. Lique, and I. R. Sims, Nat. Chem. **14**, 811 (2022).
[12] E. Herbst, R. Terzieva, and D. Talbi, MNRAS **311**, 869 (2000).
[13] M. Padovani, C. M. Walmsley, M. Tafalla, P. Hily-Blant, and G. Pineau des Forêts, Astron. Astrophys. **534**, A77 (2011).
[14] T. Hirota, S. Yamamoto, H. Mikami, and M. Ohishi, Astrophys. J. **503**, 717 (1998).
[15] F. Dumouchel, A. Faure, and F. Lique, MNRAS **406**, 2488 (2010).
[16] E. Sarrasin, D. B. Abdallah, M. Wernli, A. Faure, J. Cernicharo, and F. Lique, MNRAS **404**, 518 (2010).
[17] H. B. Niemann, S. K. Atreya, S. J. Bauer, G. R. Carignan, J. E. Demick, R. L. Frost, D. Gautier, J. A. Haberman, D. N. Harpold, D. M. Hunten, G. Israel, J. I. Lunine, W. T. Kasprzak, T. C. Owen, M. Paulkovich, F. Raulin, E. Raaen, and S. H. Way, Nature **438**, 779 (2005).
[18] H. B. Niemann, S. K. Atreya, J. E. Demick, D. Gautier, J. A. Haberman, D. N. Harpold, W. T. Kasprzak, J. I. Lunine, T. C. Owen, and F. Raulin, J. Geophys. Res. Planets **115**, E12006 (2010).
[19] J. B. Cohen and E. B. Wilson, J. Chem. Phys. **58**, 442

(1973).
[20] J. M. Bowman, Mol. Phys. **88**, 21 (1996).
[21] K. M. Christoffel and J. M. Bowman, J. Chem. Phys. **112**, 4496 (2000).
[22] R. R. Toczyłowski, F. Doloresco, and S. M. Cybulski, J. Chem. Phys. **114**, 851 (2001).
[23] F. Lique, R. Toboła, J. Kłos, N. Feautrier, A. Spielfiedel, L. F. M. Vincent, G. Chałasiński, and M. H. Alexander, Astron. Astrophys. **478**, 567 (2007).
[24] P. J. Dagdigian, Phys. Chem. Chem. Phys. **27**, 23022 (2025).
[25] T. Stoecklin, O. Denis-Alpizar, A. Clergerie, P. Halvick, A. Faure, and Y. Scribano, J. Phys. Chem. A **123**, 5704 (2019).
[26] R. A. Creswell and A. G. Robiette, Mol. Phys. **36**, 869 (1978).
[27] S. Carter, I. M. Mills, and N. C. Handy, J. Chem. Phys. **97**, 1606 (1992).
[28] G. Knizia, T. B. Adler, and H. J. Werner, J. Chem. Phys. **130**, 054104 (2009).
[29] R. A. Kendall, T. H. Dunning, and R. J. Harrison, J. Chem. Phys. **96**, 6796 (1992).
[30] D. E. Woon and T. H. Dunning, J. Chem. Phys. **98**, 1358 (1993).
[31] S. F. Boys and F. Bernardi, Mol. Phys. **19**, 553 (1970).
[32] T. M. Miller and B. Bederson, Adv. At. Mol. Phys. **13**, 1 (1978).
[33] K. A. Peterson, D. E. Woon, and T. H. Dunning, J. Chem. Phys. **100**, 7410 (1994).
[34] A. Chefai, C. Jellali, K. Hammami, and H. Aroui, Astrophys. Space Sci. **363**, 265 (2018).
[35] O. V. Egorov and A. K. Tretyakov, Russ. Phys. J. **64**, 1363 (2021).
[36] L. Tian, T. Sun, W. Zou, and X. Chen, MNRAS **545**, 1 (2026).
[37] H. J. Werner, P. J. Knowles, G. Knizia, F. R. Manby, and M. Schütz, WIREs Comput. Mol. Sci. **2**, 242 (2011).
[38] H. J. Werner, B. Follmeg, and M. H. Alexander, J. Chem. Phys. **89**, 3139 (1988).
[39] Y. Ajili and K. Hammami, Astron. Astrophys. **556**, A82 (2013).
[40] A. M. Arthurs and A. Dalgarno, Proc. R. Soc. Lond. A. Math. Phys. Sci. **256**, 540 (1960).
[41] S. Green, J. Chem. Phys. **62**, 2271 (1975).
[42] E. Pearson, R. Creswell, M. Winnewisser, and G. Winnewisser, Z. Naturforsch. A **31**, 1394 (1976).
[43] A. G. Maki, J. Phys. Chem. Ref. Data **3**, 619 (1974).
[44] J. M. Hutson and C. R. Le Sueur, Comput. Phys. Commun. **241**, 9 (2019).
[45] D. E. Manolopoulos, J. Chem. Phys. **85**, 6425 (1986).
[46] M. H. Alexander and D. E. Manolopoulos, J. Chem. Phys. **86**, 2044 (1987).
[47] K. M. Walker, F. Lique, F. Dumouchel, and R. Dawes, MNRAS **466**, 831 (2017).

DOI: 10.1063/1674-0068/cjcp2601003